Available online at www.sciencedirect.com
ScienceDirect
Physica B 403 (2008) 2008–2014
PHYSICA B
www.elsevier.com/locate/physb

# Thickness dependence of microstructures in $La_{0.9}Sr_{0.1}MnO_3$ thin films grown on exact-cut and miscut $SrTiO_3$ substrates

Hong-Di Zhang[a,b,*], Yu-Kai An[b], Zhen-Hong Mai[b], Hui-Bin Lu[b], Kun Zhao[b], Guo-Qiang Pan[c], Rui-Peng Li[c], Rong Fan[c]

[a] *Department of Applied Physics, College of Science, Tianjin University of Commerce, Tianjin 300134, PR China*
[b] *Beijing National Laboratory for Condensed Matter Physics, Institute of Physics, Chinese Academy of Sciences, Beijing 100080, PR China*
[c] *National Synchrotron Radiation Facility, University of Science and Technology of China, HeFei 230026, PR China*

Received 9 October 2006; received in revised form 8 November 2007; accepted 16 November 2007

## Abstract

The thickness dependence of microstructures of $La_{0.9}Sr_{0.1}MnO_3$ (LSMO) thin films grown on exact-cut and miscut $SrTiO_3$ (STO) substrates, respectively, was investigated by high-angle X-ray diffraction (HXRD), X-ray small-angle reflection (XSAR), X-ray reciprocal space mapping and atomic force microscopy (AFM). Results show that the LSMO films are in pseudocubic structure and are highly epitaxial [0 0 1]-oriented growth on the (0 0 1) STO substrates. The crystalline quality of the LSMO film is improved with thickness. The epitaxial relationship between the LSMO films and the STO substrates is $[0\,0\,1]_{LSMO} \| [0\,0\,1]_{EXACT\text{-}STO}$, and the LSMO films have a slight mosaic structure along the $q_x$ direction for the samples grown on the exact-cut STO substrates. However, an oriented angle of about 0.24° exists between $[0\,0\,1]_{LSMO}$ and $[0\,0\,1]_{MISCUT\text{-}STO}$, and the LSMO films have a mosaic structure along the $q_z$ direction for that grown on the miscut STO substrates. The mosaic structure of both groups of the samples tends to reduce with thickness. The diffraction intensity of the (0 0 4) peaks increases with thickness of the LSMO film. The XSAR and AFM observations show that for both groups, the interface is sharp and the surface is rather smooth. The mechanism was discussed briefly.

*PACS:* 68.55.Jk; 61.10.Nz; 81.15.Fg; 68.35.Ct

*Keywords:* Microstructures; Oriented growth; Surface morphology

## 1. Introduction

Ever since the discovery of colossal magnetoresistance (CMR) in perovskite manganese oxides, there has been a focus of active research on these kinds of materials associated with magnetic, electrical, and optical properties [1–4]. As is known, the properties mentioned above are sensitive to the structure of manganite perovskite $La_{1-x}A_x MnO_3$, where A is a divalent alkali metal ion. $La_{1-x}A_x MnO_3$ has an orthorhombic distorted perovskite structure. This structure is in lower symmetry compared to the ideal cubic perovskite, which is attributed to John–Teller distortion of the $O_6$ octahedron surrounding the Mn-ions. The occurrence of CMR behavior and magnetic properties is attributed to the presence of the disorder in the epitaxial films and the lattice strain between the film and substrate. The effect of thickness of a $La_{0.9}Sr_{0.1}MnO_3$ (LSMO) thin film and the miscut substrate on the microstructures and the strain distribution inside the films is an important parameter for potential device applications.

It has been reported that some physical properties of manganite perovskite films are dependent on different growth orientations. For example, the magnetic anisotropy [5], magnetoresistance (MR) and electrical resistivity [6] show crystalline anisotropy in epitaxial single-crystal films. Studies have been done for high-quality films like $YBa_2Cu_3O_7$, $Sr_{1-x}Ca_xRuO_3$ and $(La,Sr)_2CuO_4$ on miscut

---

*Corresponding author at: Department of Applied Physics, College of Science, Tianjin University of Commerce, Tianjin 300134, PR China. Tel.: +86 10 82649552.

*E-mail address:* hongdi_zhang@163.com (H.-D. Zhang).

0921-4526/$ - see front matter © 2007 Elsevier B.V. All rights reserved.
doi:10.1016/j.physb.2007.11.009

substrates [7–10]. Results indicated that the miscut substrates induce the formation of preferential orientation and can enhance their physical properties [11]. Report [12] has shown that the LCMO thin films deposited on tilted $SrTiO_3$ (STO) substrate possess high sensitivity of photovoltage and photocurrent. It suggests the promising potential of manganite oxide thin film as a new type of optical detectors. In this paper we further studied the thickness dependence of the microstructures and the surface morphology of LSMO films on exact-cut or/and miscut STO substrates by using X-ray and atomic force microscopy (AFM), respectively. The results obtained would be beneficial for preparing high-quality LSMO films on STO.

## 2. Experimental details

The LSMO films with different thicknesses were deposited on exact-cut and miscut STO (0 0 1) substrates, respectively, using computer-controlled laser molecular beam epitaxy [13–16]. An *in-situ* reflection high-energy electron diffraction (RHEED) and charge-coupled device (CCD) camera provide us with useful information on the crystal structure and morphology of a growing film surface. The RHEED intensity oscillation was used to exactly control the number of molecular layers. The process was carried out in an atomic oxygen gas (~20% O) at $4 \times 10^{-4}$ Pa. The substrate temperature was maintained at 620 °C during the process. The laser wavelength was 308 nm, the pulse frequency was 2 Hz and the energy density was ~1 J/cm$^2$. The films were annealed for 15 min in atomic oxygen of $2 \times 10^{-2}$ Pa after deposition, in order to remove the oxygen deficiency. Two series of LSMO films were prepared with thicknesses of 40, 20, 8, 4 and 2 nm, respectively. The first group is labeled as A–E, grown on the exact-cut STO (0 0 1) substrates and the second group is labeled as F–J, grown on the STO (0 0 1) substrates with a miscut angle of 10° towards the [1 0 0] direction of STO.

The high-angle X-ray diffractions (HXRD) were measured at the X-ray diffraction and Scattering Station in the National Synchrotron Radiation Laboratory (NSRF). The X-ray with a wavelength of 0.129 nm was used. A 0.6 mm slit was positioned before the sample, and an ion chamber behind the slit was used to monitor the intensity of the incident beam. A NaI scintillator behind the diffraction slit (0.2 mm in width) was applied to collect the intensity information reflected/scattered from the sample. The ratio of counting coefficients of the two detectors was calibrated by measuring the incident X-ray beam intensity without sample.

The X-ray small-angle reflection (XSAR) measurements and the X-ray reciprocal space mapping were performed on a high-resolution X-ray diffractometer (Bruker D8 Advance) at room temperature with Cu-K$_{\alpha 1}$ radiation. The incidence slit was 0.2 mm and that of the detector was also 0.2 mm. The experimental data of reflectivity were simulated theoretically using matrix formulation, based on the Fresnel's law in classical optics [17,18].

The surface morphology of the films was characterized by AFM on a Nano Scope IIIa, scanning probe microscope (DI Company, USA) in contact mode.

## 3. Results and discussion

### 3.1. The orientation and the lattice parameters

Fig. 1(a) shows the HXRD profiles of samples A–E deposited on exact-cut STO (0 0 1) substrates, and Fig. 1(b) is those of the second group of films deposited on miscut STO substrates. Only the (0 0 4) diffraction peaks of LSMO on STO (0 0 1) are observed, without diffraction peaks due to random crystallographic orientation or secondary phases. This reveals that the LSMO films are highly epitaxial [0 0 1]-oriented growth on the STO substrates. The diffraction intensity of the (0 0 4) peaks increases with thickness of the films.

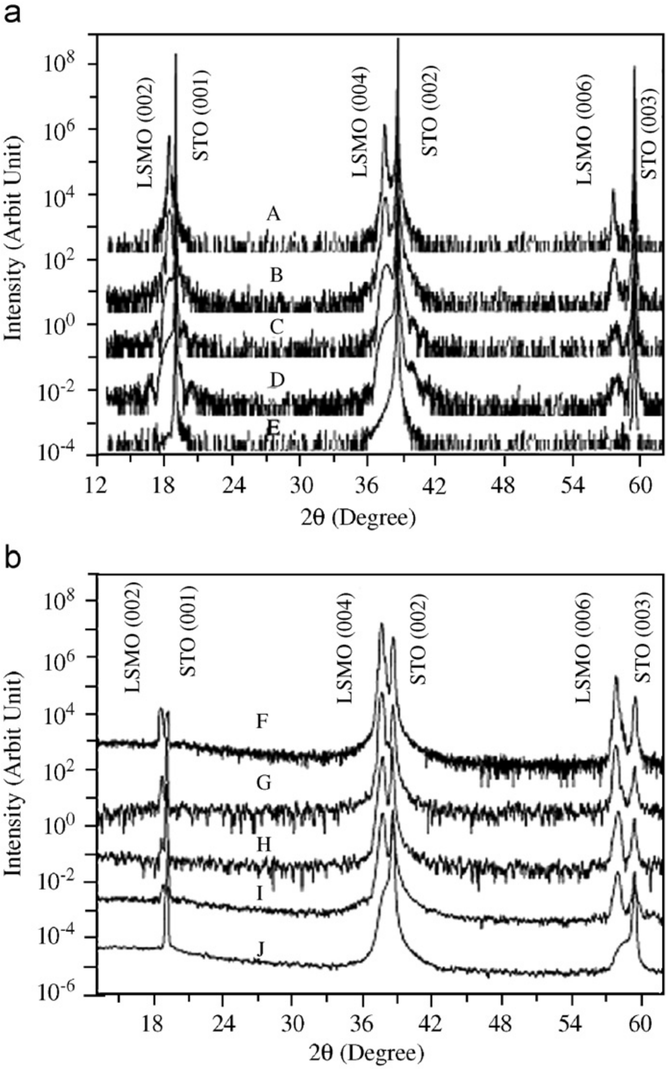

Fig. 1. High-angle X-ray diffraction of the LSMO films: (a) grown on exact-cut STO and (b) on miscut STO.

The full-width at half-maximum (FWHM) of the (0 0 4) diffraction peak rocking curve were measured for all LSMO films. Fig. 2 shows the FWHM of the (0 0 4) LSMO peaks vs film thickness. It seems that the FWHM becomes narrow with thickness, for samples A–D and F–I. The FWHMs of the (0 0 4) LSMO peaks on exact STO are about 0.25–0.35°, while those on miscut STO are about 0.06–0.075°. It is obvious that the FWHM of the (0 0 4) LSMO peaks on miscut STO was much narrower than that on exact STO. On the other hand, Zhao and co-workers [12] has reported that the electric–optical properties of the LCMO films on miscut STO are much better than those on the exact-cut one. The FWHMs of the samples E and J with the thinnest LSMO film (2 nm) are not included, because these LSMO films are so thin that most diffraction originates from the substrates. Furthermore, the film diffraction intensity of samples F–J is about 10 times stronger than that of samples A–E (as shown in Fig. 1). The above results indicate the crystalline quality of the LSMO films on miscut substrates is superior to those on exact-cut ones.

According to crystallography, the lattice parameters of the LSMO film as a pseudo-cubic structure could be determined uniquely from the positions of the (0 0 *l*), (0 *k l*) and (*h k l*) peaks. Therefore different diffraction peaks were measured for each sample, for instance (0 0 4), (0 2 6) and (2 2 4), respectively. The measurements were performed on a six-circle diffractometer at the X-ray Diffraction and Scattering Station in the NSRF. Fig. 3 shows the (0 0 4), (0 2 6) and (2 2 4) peaks of samples A and F, respectively. The behavior of diffraction profiles for the other samples is

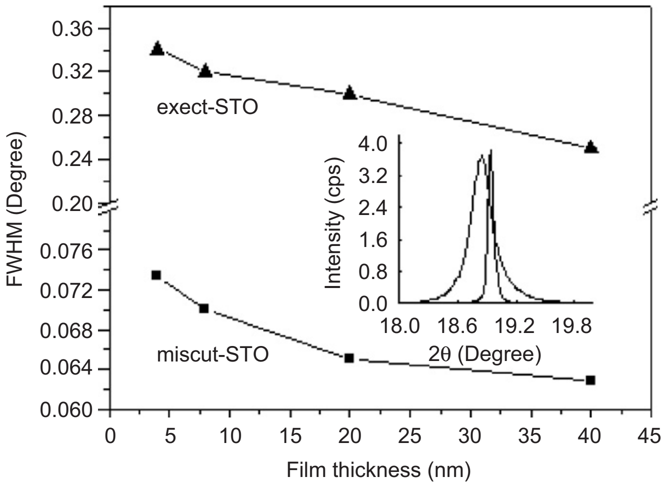

Fig. 2. The FWHM of the LSMO film (0 0 4) diffraction peaks for both groups of samples. Inset: 1 represents the rocking curve of (0 0 4) diffraction of sample A and 2 represents that of sample F.

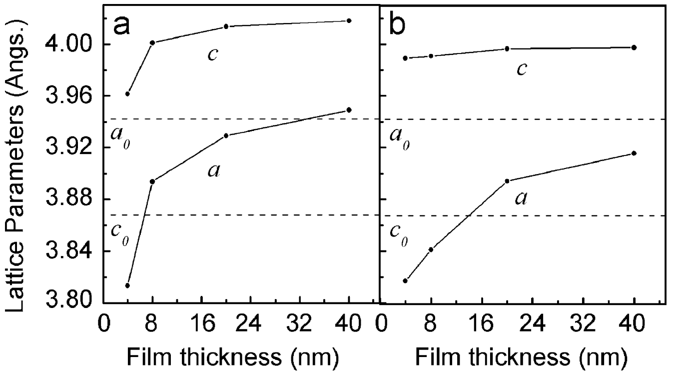

Fig. 4. Dependence of film thickness on the lattice parameters, $a_0$ and $c_0$ are the lattice parameters of the LSMO single crystal: (a) grown on the exact-cut STO and (b) on the miscut STO.

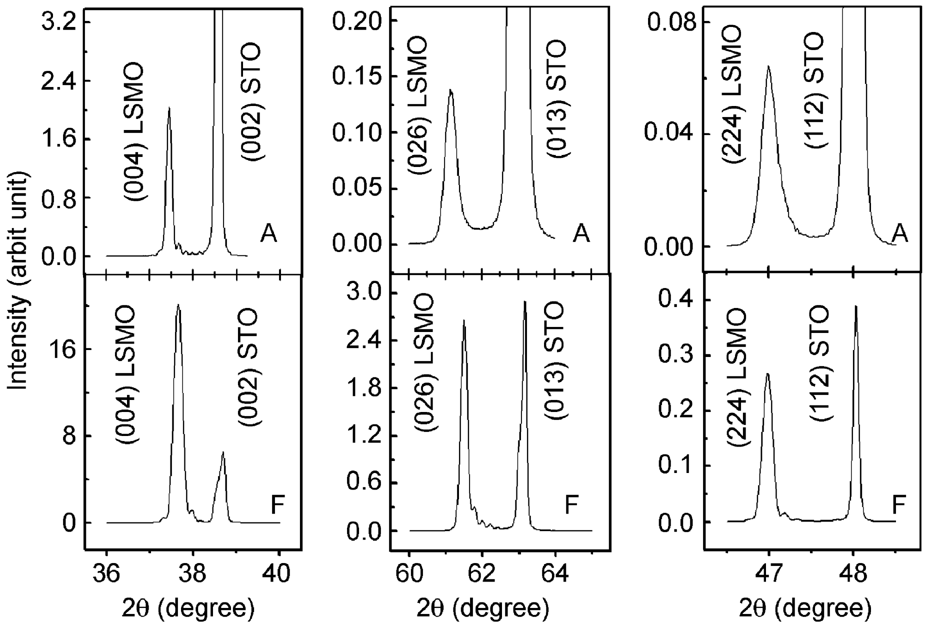

Fig. 3. X-ray diffraction profiles of the pseudocubic (0 0 4), (0 2 6) and (2 2 4) peaks of the LSMO films for samples A and F.

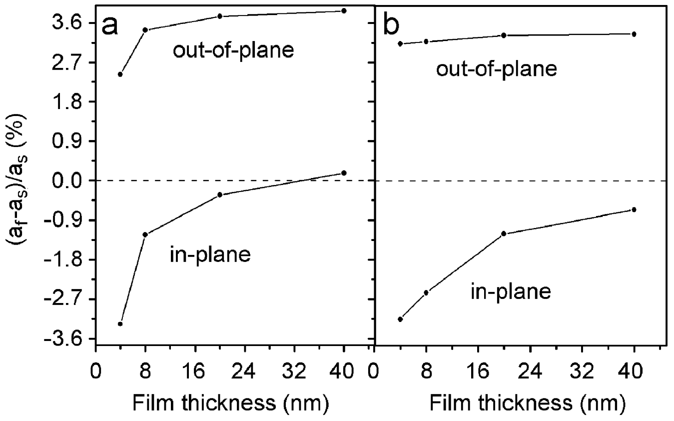

Fig. 5. The values of the strain $\varepsilon$ as a function of the film thickness: (a) samples A–D and (b) samples F–I.

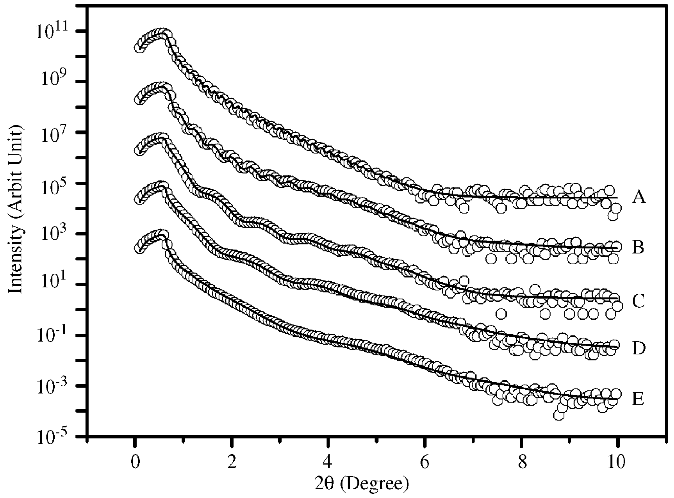

Fig. 6. Experimental and theoretical profiles of XSAR for samples A–E. The circle represents the experiment curve and the solid line is the fitting curve, respectively.

similar to Fig. 3. This result suggests that the LSMO thin films have a pseudocubic structure with a perovskite unit cell.

Fig. 4 shows the lattice parameters as a function of the thickness for the samples A–D and F–I. Samples E and J were ignored in Fig. 4 because the films are too thin to be detected. STO is a perfect cubic perovskite structure with a lattice parameter of $a = 0.3905$ nm. LSMO is a distorted perovskite structure, exhibiting an orthorhombic variant. Its lattice parameters in bulk form at room temperature are: $a = 0.5469$ nm, $b = 0.556033$ nm, $c = 0.77362$ nm [19], respectively. On the other hand, the LSMO/STO system can be considered as a pseudocubic, whose lattice parameters are $a^* = b^* = \sqrt{a^2 + b^2} = 0.78844$ nm and $c^* = c = 0.77362$ nm, reducing the growth energy. In the paper, the lattice parameters of $a_0 = b_0 = \frac{1}{2}a^* = 0.39422$ nm and $c_0 = \frac{1}{2}c^* = 0.38681$ nm for LSMO films were used to illustrate the lattice mismatch of the system. The in-plane, as well as the out-of-plane lattice parameters increase with film thickness (see Fig. 4). The values of the strain $\varepsilon$ were plotted as the function of film thickness, according to the formula $\varepsilon = (a_f - a_R)/a_R$, where $a_f$ is the lattice parameter of the LSMO films and $a_R$ that of the completely relaxed (unstrained) single crystal (in Fig. 5). It seems that the LSMO film undergoes an in-plane compressive stress leading to a larger out-of-plane lattice parameter $c$ due to the tetragonal distortion. Therefore, the out-of-plane has a tensile strain. In Fig. 5, as film thickness increases, the samples F–I show similar behaviors with that of samples A–D.

### 3.2. Surface and interface

To investigate the surface and interface structure of the LSMO films, the XSAR was used on these 10 samples.

Table 1
Theoretical simulation results of the X-ray small-angle reflectivity curves

| Sample | Nominal thickness | Layers | Thickness (±1 Å) | Surface and interface roughness (±1 Å) | Density (±0.001 atoms/Å$^3$) |
|---|---|---|---|---|---|
| A | 400 | $La_{0.9}Sr_{0.1}MnO_3$ | 23 | $\sigma_{air/cap} = 5$ | 0.078 |
| | | $La_{0.9}Sr_{0.1}MnO_3$ | 418 | $\sigma_{LSMO/STO} = 3$ | 0.08 |
| | | $SrTiO_3$ | – | $\sigma_{LSMO/STO} = 6.5$ | 0.084 |
| B | 200 | $La_{0.9}Sr_{0.1}MnO_3$ | 20 | $\sigma_{air/cap} = 4$ | 0.072 |
| | | $La_{0.9}Sr_{0.1}MnO_3$ | 191 | $\sigma_{cap/LSMO} = 2.8$ | 0.08 |
| | | $SrTiO_3$ | – | $\sigma_{LSMO/STO} = 6$ | 0.084 |
| C | 80 | $La_{0.9}Sr_{0.1}MnO_3$ | 18 | $\sigma_{air/cap} = 3.5$ | 0.07 |
| | | $La_{0.9}Sr_{0.1}MnO_3$ | 69 | $\sigma_{cap/LSMO} = 3$ | 0.08 |
| | | $SrTiO_3$ | – | $\sigma_{LSMO/STO} = 6$ | 0.084 |
| D | 40 | $La_{0.9}Sr_{0.1}MnO_3$ | 10 | $\sigma_{air/cap} = 3$ | 0.074 |
| | | $La_{0.9}Sr_{0.1}MnO_3$ | 50 | $\sigma_{cap/LSMO} = 2$ | 0.08 |
| | | $SrTiO_3$ | – | $\sigma_{LSMO/STO} = 5$ | 0.084 |
| E | 20 | $La_{0.9}Sr_{0.1}MnO_3$ | 4 | $\sigma_{air/cap} = 2.8$ | 0.076 |
| | | $La_{0.9}Sr_{0.1}MnO_3$ | 24 | $\sigma_{cap/LSMO} = 3$ | 0.08 |
| | | $SrTiO_3$ | – | $\sigma_{LSMO/STO} = 4$ | 0.084 |

XSAR is sensitive to the electron density and interfacial roughness between layers in multilayer structure. Through simulating the experimental results, the atomic density, the thickness of each layer and the roughness (RMs) of the interface and the surface of the LSMO layer will be obtained. Fig. 6 shows the experimental and theoretical profiles of the XSAR for the first group. The peaks on the reflection curves reveal that the interfaces of the samples are quite sharp, shown in Fig. 6. The period of their diffraction peaks decrease with thickness. The XSAR profiles of the second group show the same tendency as those in Fig. 6. This means that the layer behavior of the second group of samples is similar to that of the first group of samples.

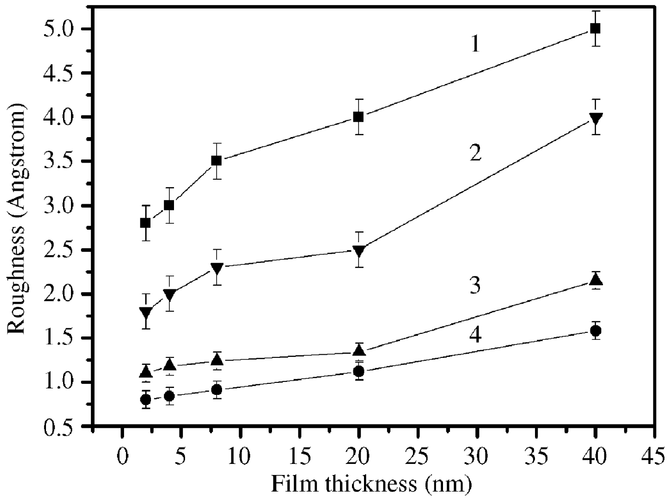

Fig. 7. Dependence of the film thickness on the LSMO film surface roughness. Lines 1 and 2 were measured by X-ray reflection for the sample grown on exact- and miscut STO, respectively. Lines 3 and 4 measured by AFM, respectively.

According to the best-fitting parameters of the theoretical simulation listed in Table 1 the nominal thickness of the LSMO layer for all samples seems to deviate slightly from the real thickness. It might be attributed to the fluctuations of deposition condition during the process. The LSMO films are quite smooth, whose surface roughness is about one single cell. This result is in agreement with that of the AFM measurement (as shown in Fig. 7). Both the surface and interface roughness of the LSMO/STO system increases with thickness. There exists a non-designed cap layer on the upper surface of the sample and its density is different from that of the LSMO film. The thickness of the cap layer also increases with thickness. This non-designed cap layer might be caused by surface oxidation, since the thicker the LSMO film, the longer the depositing time.

Fig. 7 shows the dependence of the surface roughness on the film thickness. The surface roughness of the LSMO films is about one single cell. It means that the surface of both the groups is rather smooth. Moreover, the second group is a little smoother than that of the first group. This

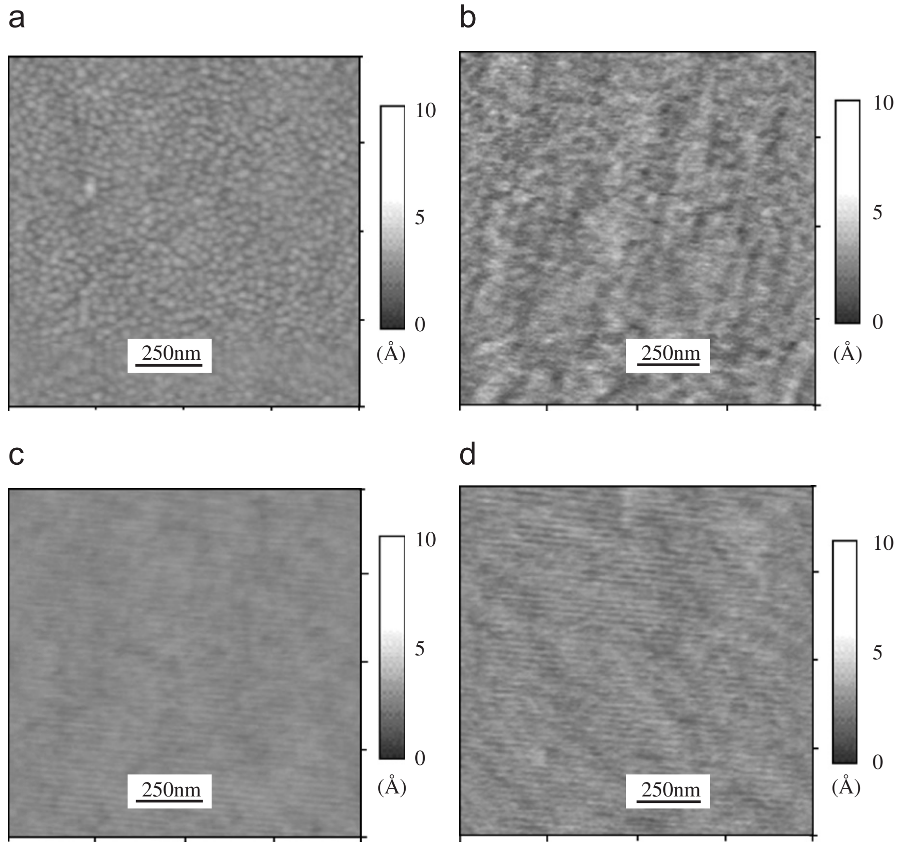

Fig. 8. The AFM images of the samples A, E, F and J: (a) sample A, (b) sample E, (c) sample F and (d) sample J.

result is supported by AFM observation shown on lines 3 and 4 in Fig. 7. The surface roughness values determined by XSAR and AFM are different because the former characterizes the roughness of the under layer, while the latter just indicates the surface. Meanwhile, the area measured by XSAR is millimeter square, about thousand times larger than that of AFM (about micron square). After all, the tendency of the relation between the surface roughness and the layer thickness measured by the both methods is similar.

The surface morphology was examined by AFM, shown in Fig. 8. As film thickness increases, the surface morphology of the LSMO films is generally smooth in atom level. It indicates that the LSMO films were grown epitaxially layer by layer on the STO substrate. The crystalline grains appear on the surface of the samples grown on the exact-cut STO with increasing thickness. The surface for the film on miscut STO is smoother than that on exact-cut STO.

### 3.3. Reciprocal space mapping

To obtain more details of the microstructural information of the films, the X-ray reciprocal space mapping around the (0 0 4) reciprocal lattice point of the STO substrate were examined for both groups. As is known, the distribution of the X-ray diffraction intensities in the X-ray reciprocal space mapping provides information about the misorientation, lattice mismatch, mosaic structure and relaxation of the epitaxial films.

Fig. 9 shows the X-ray reciprocal space mapping of the samples A–C and F–H. It reveals that the LSMO films are epitaxial [0 0 1]-oriented growth on the (0 0 1) STO substrates. For samples on exact-cut STO substrate, no misorientation between the film and substrate system was detected, that is $[001]_{\mathrm{LSMO}} \| [001]_{\mathrm{EXACT\text{-}STO}}$. The LSMO films show a slight mosaic structure along the $q_x$ direction, and the mosaic degree tends to decrease with thickness. On the contrary, for films on miscut STO substrates, the (0 0 1) peak was not parallel to that of miscut-STO. There exists an epitaxial angle between $[001]_{\mathrm{LSMO}}$ and $[001]_{\mathrm{MISCUT-STO}}$ shown in Fig. 9(d–f) respectively. The LSMO films have a mosaic structure along the $q_z$ direction. It might be caused by the strain relaxation along the $q_z$ direction. The behavior of the X-ray reciprocal mapping around the (0 0 4) reciprocal lattice point for STO substrate of the other samples are similar to that shown in Fig. 9. According to the positions of the reciprocal lattice points

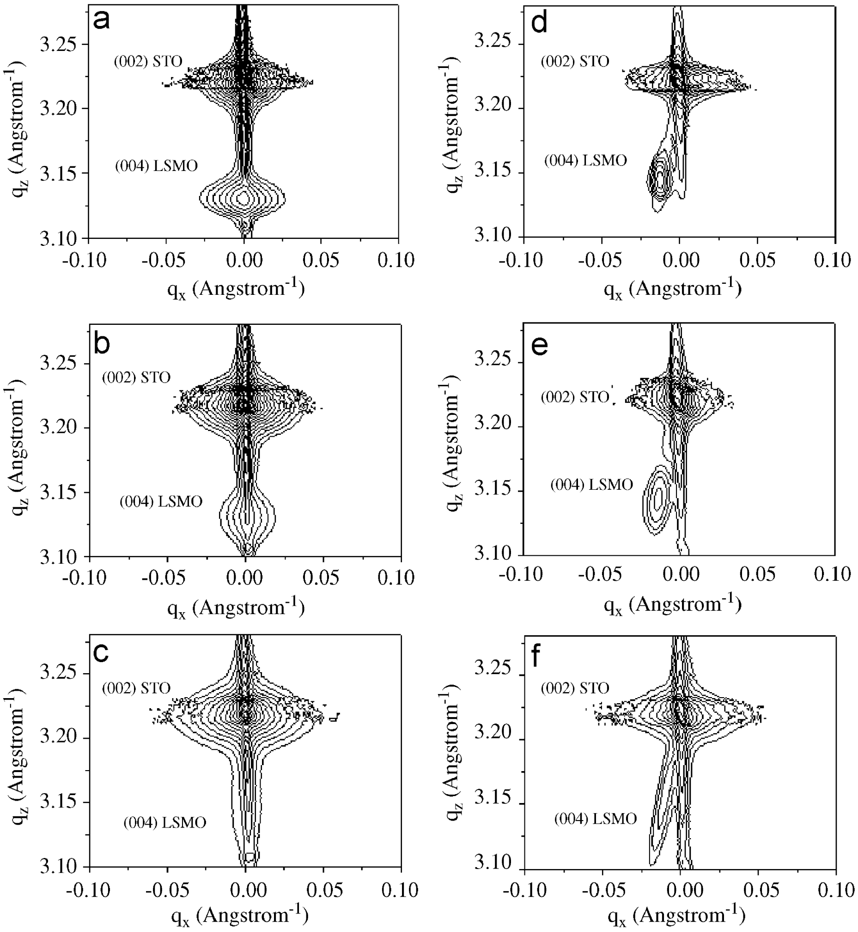

Fig. 9. X-ray reciprocal space mapping: (a) sample A, (b) sample B, (c) sample C, (d) sample F, (e) sample G and (f) sample H.

of the LSMO/STO system in Fig. 9, the $q_x$ and $q_z$ values of LSMO film were determined. They are, respectively, (0, 3.129) for sample A, (0, 3.132) for sample B, (−0.012, 3.145) for sample F, (−0.0137, 3.143) for sample G, and (0, 3.22) for STO substrate. An epitaxial angle ($\theta$) between $[0\,0\,1]_{\mathrm{LSMO}}$ and $[0\,0\,1]_{\mathrm{MISCUT\text{-}STO}}$ can be calculated as about 0.24° ($\arctan\theta = q_{x\text{-LSMO}}/q_{z\text{-LSMO}}$). The lattice mismatch ($\delta$) between the LSMO/STO systems can be calculated according to:

$$\delta = \frac{q_{z\text{-STO}} - q_{z\text{-LSMO}}}{q_{z\text{-LSMO}}}.$$

Therefore the lattice mismatch for the LSMO on the miscut STO is about 2.4%, which is smaller than that on exact-cut STO (2.8%). The LSMO films of both groups grew along the [0 0 1]-orientation, in agreement with the XRD results shown in Fig. 1. There exists a mosaic structure in certain regions for the LSMO/exact STO system and a misorientation for LSMO/miscut STO system, which can be understood by the lattice modulated to minimize strain.

## 4. Conclusion

Thickness dependence of microstructures in LSMO thin films grown on exact-cut or/and miscut STO substrates, respectively, was investigated by several X-ray diffraction techniques and AFM. The results reveal that the LSMO films show a pseudocubic structure and are highly epitaxial [0 0 1]-oriented growth on STO. The epitaxial relationship between the LSMO films and STO substrates is $[0\,0\,1]_{\mathrm{LSMO}\text{-}}\|_{[0\,0\,1]\mathrm{EXACT\text{-}STO}}$ , and the LSMO film has a slight mosaic structure along the $q_x$ direction for the films on the exact-cut STO. However, an angle of about 0.24° exists between $[0\,0\,1]_{\mathrm{LSMO}}$ and $[0\,0\,1]_{\mathrm{MISCUT\text{-}STO}}$, and the LSMO film has a mosaic structure along the $q_z$ direction for those on miscut STO. The degree of mosaic structure for both groups decreases with thickness. The diffraction intensity of the film {0 0 2} peaks increases with thickness. The crystalline quality of LSMO on miscut STO is better than that on exact-cut ones. XSAR and AFM observations show the interface is sharp and the surface is rather smooth for all samples measured. The results obtained would be benefit to grow high-quality LSMO film on STO substrate.

## Acknowledgment

This work was supported by the National Natural Science Foundation of China (Grant nos. 10274096 and 10574159).

## References

[1] S. Jin, T.H. Tiefel, M. Mccormack, R.A. Fastnacht, R. Ramesh, L.H. Chen, Science 264 (1994) 413.
[2] S. Jin, T.H. Tiefel, M. Mccormack, H.M. Obryan, L.H. Chen, R. Ramesh, D. Schurig, Appl. Phys. Lett. 67 (1995) 557.
[3] W.J. Gallagher, S.S.P. Parkin, Y. Lu, X.P. Bian, A. Marley, K.P. Roche, R.A. Altman, S.A. Rishton, C. Jahnes, T.M. Shaw, G. Xiao, J. Appl. Phys. 81 (1997) 3741.
[4] J. Jorzick, O. Demokritov, B. Hillebrands, B. Bartenlian, C. Chappert, D. Decanini, F. Rousseaux, E. Cammbril, Appl. Phys. Lett. 75 (1999) 3859.
[5] F. Tsui, M.C. Smoak, T.K. Nath, C.B. Eom, Appl. Phys. Lett. 76 (2000) 2421.
[6] V.S. Amaral, A.A.C.S. Lourenco, J.P. Araújo, P.B. Tavares, E. Alves, J.B. Sousa, J.M. Vieira, M.F. da Silva, J.C. Soares, J. Magn. Magn. Mater. 211 (2000) 1.
[7] D.H. Lowndes, X.Y. Zheng, S. Zhu, J.D. Budai, R.J. Warmack, Appl. Phys. Lett. 61 (1992) 852.
[8] D.G. Schlom, D. Angelmetti, J.D. Bednorz, R.F. Broom, A. Catana, T. Frey, C. Gerber, H.J. Guntherodt, H.P. Lang, J. Mannhart, Z. Phys. B 86 (1992) 163.
[9] C.B. Eom, R.J. Cava, R.M. Fleming, J.M. Phillips, R.B. van Dover, J.H. Marshall, J.W.P. Hsu, J.J. Krajewski, W.F. Peck Jr., Science 258 (1992) 1766.
[10] J. Kwo, R.M. Fleming, H.L. Kao, D.J. Werder, C.H. Chen, Appl. Phys. Lett. 60 (1992) 1905.
[11] M. Fatemi, A.E. Wickenden, D.D. Koleske, M.E. Twigg, J.A. Freitas Jr., R.L. Henry, R.J. Gorman, Appl. Phys. Lett. 73 (1998) 608.
[12] K. Zhao, K.J. Jin, Y.H. Huang, H.B. Lu, M. He, Z.H. Chen, Y.L. Zhou, G.Z. Yang, Physica B 373 (2006) 72.
[13] Y.H. Huang, M. He, K. Zhao, H.F. Tian, H.B. Lu, K.J. Jin, Z.H. Chen, Y.L. Zhou, J.Q. Li, G.Z. Yang, Chin. Phys. Lett. 22 (11) (2005) 2950.
[14] X.B. Lu, H.B. Lu, Z.H. Chen, X. Zhang, R. Huang, H.W. Zhou, X.P. Wang, B.Y. Nguyen, C.Z. Wang, W.F. Xiang, M. He, B.L. Cheng, Appl. Phys. Lett. 85 (16) (2004) 3543.
[15] F. Chen, H.B. Lu, T. Zhao, R.P. Wang, Y.L. Zhou, Z.H. Chen, G.Z. Yang, Sci. China Ser. A 44 (7) (2001) 947.
[16] G.Z. Yang, H.B. Lu, F. Chen, T. Zhao, Z.H. Chen, J. Cryst. Growth 227 (2001) 929.
[17] L.G. Parratt, Phys. Rev. 95 (1954) 359.
[18] G.M. Luo, M.L. Yan, Z.H. Mai, W.Y. Lai, Y.T. Wang, Phys. Rev. B 56 (1997) 3290.
[19] D.E. Cox, T. Iglesias, E. Moshopoulou, K. Hirota, K. Takahashi, Y. Endoh, Phys. Rev. B 64 (2001) 024431.